Geochemistry, Geophysics, Geosystems

RESEARCH ARTICLE
10.1029/2018GC007588

In Situ Characterization of the Lithosphere-Asthenosphere System beneath NW Pacific Ocean Via Broadband Dispersion Survey With Two OBS Arrays

Akiko Takeo[1], Hitoshi Kawakatsu[1], Takehi Isse[1], Kiwamu Nishida[1], Hajime Shiobara[1], Hiroko Sugioka[2], Aki Ito[3], and Hisashi Utada[1]

[1]Earthquake Research Institute, The University of Tokyo, Tokyo, Japan, [2]Graduate School of Science, Kobe University, Kobe, Japan, [3]Department of Deep Earth Structure and Dynamics Research, Japan Agency for Marine, Earth Science and Technology, Yokosuka, Japan

Key Points:
- Broadband ocean bottom seismic observation is conducted in the NW Pacific Ocean at two sites with seafloor ages of 130 and 140 Ma
- Significant seismic velocity variation in the LVZ of two areas is revealed that may indicate the presence of small-scale convection
- Azimuthal anisotropy depth profiles indicate that the fast directions do not necessarily coincide with the ancient spreading directions

Correspondence to:
A. Takeo,
akiko-t@eri.u-tokyo.ac.jp

Citation:
Takeo, A., Kawakatsu, H., Isse, T., Nishida, K., Shiobara, H., Sugioka, H., et al. (2018). In situ characterization of the lithosphere-asthenosphere system beneath NW Pacific Ocean via broadband dispersion survey with two OBS arrays. *Geochemistry, Geophysics, Geosystems*, *19*. https://doi.org/10.1029/2018GC007588

Received 2 APR 2018
Accepted 6 SEP 2018
Accepted article online 11 SEP 2018

Abstract We conducted broadband dispersion survey by deploying two arrays of broadband ocean bottom seismometers in the northwestern Pacific Ocean at seafloor ages of 130 and 140 Ma. By combining ambient noise and teleseismic surface wave analyses, dispersion curves of Rayleigh waves were obtained at a period range of 5–100 s and then used to invert for one-dimensional isotropic and azimuthally anisotropic β_V (V_{SV}) profiles beneath each array. The obtained profiles show ~2% difference in isotropic β_V in the low-velocity zone (LVZ) at a depth range of 80–150 km in spite of the small difference in seafloor ages and the horizontal distance of ~1,000 km. Forward dispersion-curve calculation for thermal models indicates that simple cooling models cannot explain the observed difference and an additional mechanism, such as sublithospheric small-scale convection, is required. In addition, the fastest azimuths of azimuthal anisotropy in the LVZ significantly deviate from the current plate motion direction. We infer that these observations are consistent with the presence of small-scale convection beneath the study area. As for azimuthal anisotropy in the Lid, the peak-to-peak intensity is 3–4% at the depth from Moho to ~40 km. The fastest direction is almost perpendicular to magnetic lineation in area A at 130 Ma and oblique to magnetic lineations in area B at 140 Ma, suggesting complex mantle flow beneath the infant Pacific Plate surrounded by three ridge axes. The intensity of azimuthal anisotropy in the LVZ is ~2%, indicating that radial anisotropy is stronger than azimuthal anisotropy therein.

1. Introduction

The theory of plate tectonics has been widely accepted to explain surface features such as the lineations of magnetic anomalies (Vine & Matthews, 1963) and the increase of sea depth with seafloor age caused by cooling of the lithosphere-asthenosphere system (LAS) beneath the ocean (Davis & Lister, 1974). Seismic surface-wave studies have verified the idea of cooling by obtaining uppermost mantle structure including the low-velocity zone (LVZ) and overlying Lid at different seafloor ages (Harmon et al., 2009; Maggi et al., 2006a; Nishimura & Forsyth, 1988). Recent body-wave studies revealed sharp velocity reduction between Lid and LVZ called as G-discontinuity, which is one of the candidates of the oceanic lithosphere-asthenosphere boundary (Bagley & Revenaugh, 2008; Kawakatsu et al., 2009; Kawakatsu & Utada, 2017; Kumar & Kawakatsu, 2011; Revenaugh & Jordan, 1991; Rychert & Shearer, 2011).

Although the correlation between the seafloor age and the uppermost mantle structure is clearly shown by tomography studies especially at seafloor ages younger than ~60 Ma, the deviation from average structures or the cooling models has been discussed continually (e.g., Maggi et al., 2006a; Montagner, 1985; Ritzwoller et al., 2004). Numerical studies also suggest the presence of small-scale convection (SSC) in the oceanic asthenosphere (e.g., Huang & Zhong, 2005; Richter & Parsons, 1975), which is considered to reheat the bottom of the oceanic lithosphere and causes shallower ocean depth and larger heat flow at old seafloor compared to those of the half-space cooling model. Those surface observations have been fitted by plate-cooling models with a certain plate thickness below which temperature is a constant value (Parsons & Sclater, 1977; Stein & Stein, 1992). The detailed discussion has been, however, difficult due to the limited lateral and vertical resolution of tomography models especially in the oceanic regions.

Seismic azimuthal anisotropy is another physical property that reflects ancient and/or current flow in the oceanic mantle related to plate motions. In early studies, body-wave azimuthal anisotropy below Moho

discontinuity is used to infer ridge-perpendicular flow during the seafloor spreading (Raitt et al., 1971). Surface-wave tomography studies obtained azimuthal anisotropy in the lithosphere with the fastest azimuths perpendicular to magnetic lineations and ancient ridge axes (Debayle & Ricard, 2013; Smith et al., 2004). Surface-wave studies also obtained anisotropic structures in deeper depths of up to ~200 km and showed ridge-perpendicular flow frozen in oceanic lithosphere and the flow parallel to the current plate motion in the oceanic asthenosphere (Maggi et al., 2006b; Nishimura & Forsyth, 1988; Tanimoto & Anderson, 1984). By recent seafloor observations, the complexity of flow in the uppermost mantle is also revealed from lithospheric azimuthal anisotropy oblique to ancient ridge axes (Takeo et al., 2016; Toomey et al., 2007). The similar observation in the old oceanic lithosphere apart from current ridges has not been obtained yet.

For improving our understanding of the oceanic LAS especially in the middle to old seafloor ages of 60–150 Ma, several seafloor observation projects have started in different regions in the Pacific Ocean in the 2010s almost concurrently (Baba et al., 2013; Lin et al., 2016; Shintaku et al., 2014). In this study, we show the results from surface-wave array analyses of broadband ocean bottom seismometers (BBOBSs) that we call "broadband dispersion survey," as opposed to the conventional refraction survey, conducted in the northwest Pacific Ocean under the Normal Oceanic Mantle (NOMan) project in 2010–2014.

2. Broadband Dispersion Survey Beneath the NW Pacific Ocean

Recent advances in ocean bottom broadband seismometry (e.g., Suetsugu & Shiobara, 2014), together with advances in the seismic analysis methodology (e.g., Shapiro & Campillo, 2004), have enabled us to resolve the regional one-dimensional structure of the entire LAS, including seismic anisotropy (azimuthal and, hopefully, radial), with deployments of ~10 BBOBSs (e.g., Lin et al., 2016; Takeo et al., 2013, 2014, 2016). The multiband method for the ocean-bottom broadband dispersion survey utilizes seismic surface waves at periods of 3–150 s (ambient noise for 3–30 s and teleseismic surface waves for 30–150 s or longer) recorded by arrays of BBOBSs. This broadband dispersion measurement allows us to obtain one-dimensional isotropic and anisotropic structure beneath the array from the surface to the LVZ, that is, the entire oceanic LAS, without an a priori assumption for the shallow-most structure, the assumption often made for the global surface wave tomography. We have conducted such surveys beneath the NW Pacific Ocean under the NOMan project.

2.1. Data

The NOMan project is designed to understand the oceanic LAS and the mantle transition zone in the "normal" oceanic mantle by the collaboration of seismology (Takeuchi et al., 2017) and ocean electromagnetic studies (Baba et al., 2013, 2017; Matsuno et al., 2017). There are two arrays in the northwest (area A) and southeast (area B) of the Shatsky Rise (Figure 1). The numbers of BBOBS stations are 10 and 8 for areas A and B, respectively. The instruments are BBOBS-NX (Shiobara et al., 2013) for five stations in area A, and conventional BBOBSs (cf., Suetsugu & Shiobara, 2014) for other 13 stations. The interstation distances are 100–150 km, and the array sizes are ~500 km. The observation period is from 2010 to 2014 including six different observation phases (the detail of the station information can be found at the following URL: http://ohpdmc.eri.u-tokyo.ac.jp/dataset/campaign/obs/nomantle/station/index.html).

2.2. Broadband Dispersion Analysis

We applied surface-wave array analysis methods and inversion methods for obtaining one-dimensional isotropic and azimuthally anisotropic β_V profiles in each area (Takeo et al., 2013, 2014, 2016). The shear-wave velocity, β_V, is that of a vertically polarized horizontally propagating shear wave in a radially anisotropic media defined by Takeuchi and Saito (1972), whose vertical structure mostly controls dispersion curves of Rayleigh waves. Although β_V is exactly same as V_{SV} often used by other surface-wave studies, we denote it as β_V because it can be different from the velocity of SV waves that appears in seismology textbooks and body-wave studies (Kawakatsu, 2016; Kawakatsu & Utada, 2017).

At a period range of 5–30 s, we extracted background Rayleigh waves in ambient noise by cross-correlating seismograms in each pair of stations including the fundamental-mode Rayleigh wave (0S mode) at a period range of 15–30 s and the first higher-mode Rayleigh wave (1S mode) at a period range of 5–10 s. These two modes appear because of the energy concentration of 0S mode in the water layer at periods shorter than ~15 s for the seafloor depth of ~6,000 m (e.g., Harmon et al., 2007; Yao et al., 2011). In detail, the period

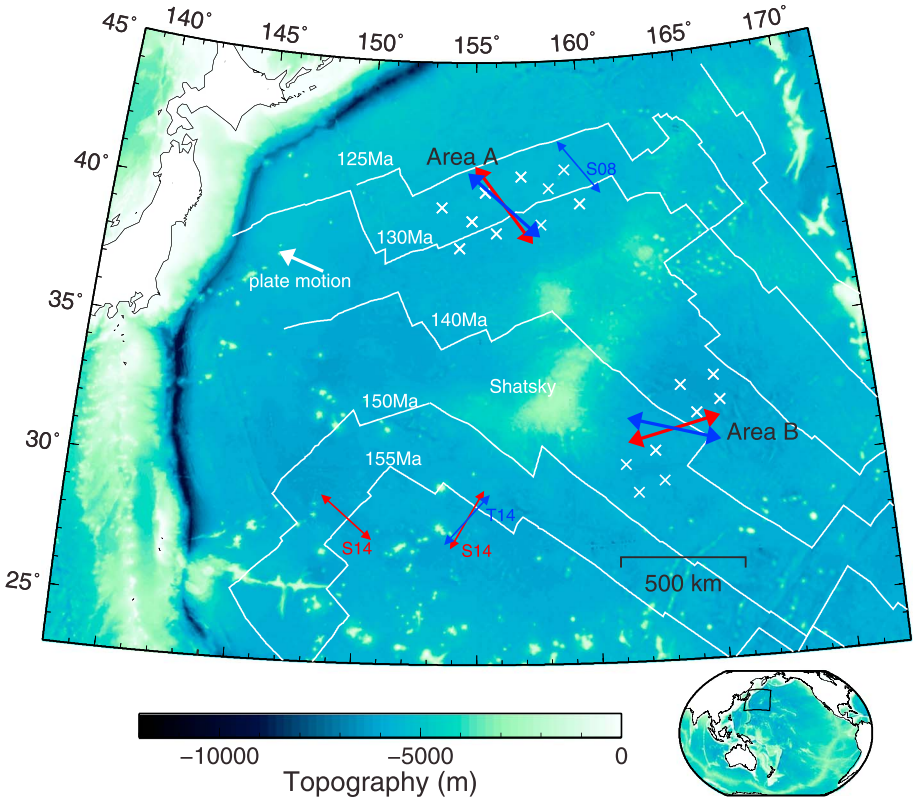

Figure 1. Map of BBOBS stations of the NOMan project marked by crosses in area A at a seafloor age of 130 Ma and area B at a seafloor age of 140 Ma that are separated by a horizontal distance of ~1,000 km. The thick arrows represent fastest azimuths at a depth shallower than ~20 km (blue) and deeper depths of ~80–100 km (red) determined in this study. The thin arrows are the azimuths at depths shallower than ~20 km (blue) and deeper depths of ~50–80 km (red) by previous studies: S08 (Shinohara et al., 2008) near area A and S14 (Shintaku et al., 2014) and T14 (Takeo et al., 2014) at southwest of the Shatsky Rise. Thin white lines indicate the seafloor age from Müller et al. (2008). The area of the large map is shown by a rectangle in the small semiglobal map at the bottom.

range of phase-velocity measurements is 8–10 s for 1S mode in area A (Figure 2a) due to lower signal-to-noise ratio at periods shorter than 8 s, probably because of the thick sediment layer in this area (Shinohara et al., 2008) creating additional mode transition at a period of ~7 s (see an example in Tonegawa et al., 2015). At a longer period range of 30–100 s, we analyzed teleseismic fundamental-mode Rayleigh waves by assuming propagation of a plane wave in a local coordinate defined by Forsyth and Li (2005). Although we analyzed Love waves, we will not describe the detail because the significant interference between higher- and fundamental- mode Love waves cannot be resolved with our dataset of small array size (e.g., Foster et al., 2014; Gaherty et al., 1996).

In the analyses of ambient noise and teleseismic waves, we measured average phase velocities (Figure 2a) and their azimuthal dependences (Figures 3a and 3b) in each area. We then inverted for one-dimensional isotropic (Figure 2b) and azimuthally anisotropic (Figures 3c and 3d) β_V models in each area by assuming one oceanic, three crustal, and nine mantle layers from sea surface to a depth of 150 km, and vertical smoothing parameters same as our previous studies (Takeo et al., 2016).

Details of methods are described in Takeo et al. (2013, 2014, 2016) with two additional improvements in phase-velocity measuring procedures in this study. For teleseismic analysis, B-spline functions are used to obtain dispersion curves in our previous studies (Takeo et al., 2013), but here we inverted for one-dimensional β_V model for each event to obtain more realistic phase-velocity measurements (model-based approach; e.g., Cara & Leveque, 1987): each β_V model has 14 independent layers from seafloor to a depth of 300 km without any vertical smoothing, and we retain only the phase-velocity measurements to invert for final models. This

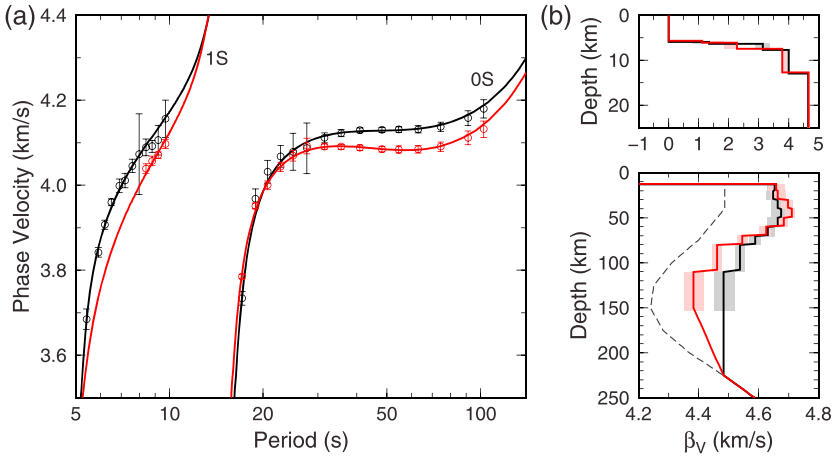

Figure 2. (a) Average phase velocities of Rayleigh waves, c_{ave}, in area A (red circles) and B (black circles) and model phase velocities (solid lines) in each area. Bone-dimensional azimuthally isotropic β_V profiles. The light shades represent one standard deviation ranges of bootstrap solutions as model uncertainties in each area. The dashed line is the ORM model by Maggi et al. (2006a) used as a reference at depths deeper than 225 km in this study. The depth of 0 km corresponds to the sea surface.

improvement provides appropriate frequency smoothing (Figure 4) and better resolution to the pattern of azimuthal anisotropy compared to B-spline expansions.

In addition, for both teleseismic and ambient noise analyses, average phase-velocity measurements (c_{ave}) are obtained by fitting phase velocities by $c_{ave}(1 + A_2 \cos 2(\theta - \phi_{max}))$, where θ is propagation azimuth, and A_2 and ϕ_{max} are intensity and fastest azimuth of azimuthal anisotropy shown in Figure 3c. If fitting of azimuthal anisotropy is not employed as previous studies (Takeo et al., 2013, 2016), bias due to azimuthal anisotropy appears in the average phase-velocity measurements especially at a period range of 30–80 s in area A (Figure 4). The degree of bias is ~1% and not negligible, unlike our previous studies, due to limited azimuthal coverage of raypaths and the NE-SW elongated array configuration in this study.

3. Results

3.1. One-Dimensional Isotropy *S* Wave Velocity Profile

In the one-dimensional β_V profile (Figure 2b), especially in area A, the velocity drops to values below 4.5 km/s at depths deeper than 80 km from values above 4.6 km/s at depths shallower than 60 km. From the large velocity contrast of ~5%, we define that the Lid and the LVZ exist at depths of 10–60 km and 80–150 km, respectively. Although the velocity contrast is smaller with a value of ~3%, we also define the Lid and LVZ at the same depth ranges in area B. As previous studies, we here simply interpret that the Lid and the LVZ correspond to the lithosphere and the asthenosphere, respectively. The bottom of LVZ is not well defined due to the limited period range of dispersion measurements and linear interpolation of velocity structure at a depth range of 80–150 km in this study. It should be noted that rather constant velocities are observed between depths of 10 and ~60 km in two areas, indicating a Lid-like structure that is also seen in our earlier study beneath the Philippine Sea (Takeo et al., 2013). The depth of Lid-to-LVZ transition is also of a recent interest (e.g., Burgos et al., 2014; Yoshizawa, 2014); the largest changes occur around a depth range of 60–80 km in both areas. The amplitude of the velocity reduction from the Lid to the LVZ in total is estimated to be ~6.5% and ~3.7% in A and B areas, respectively.

3.2. Azimuthal Anisotropy Profile

The azimuthal dependence of phase velocity could be clearly observed for the analysis of ambient noise and teleseismic waves (Figures 3a and 3b) both for the 1S mode at periods of 5–10 s and for the 0S mode at periods of 17–50 s (Figure 3c). The inverted one-dimensional profiles have strong azimuthal anisotropy of 3–4% at depths of 10–40 km in the top ~30 km of the mantle, and smaller anisotropy of 2% at deeper depths (Figure 3d). The azimuth of maximum β_V is NW-SE in area A and WNW-ESE in area B, which is slightly

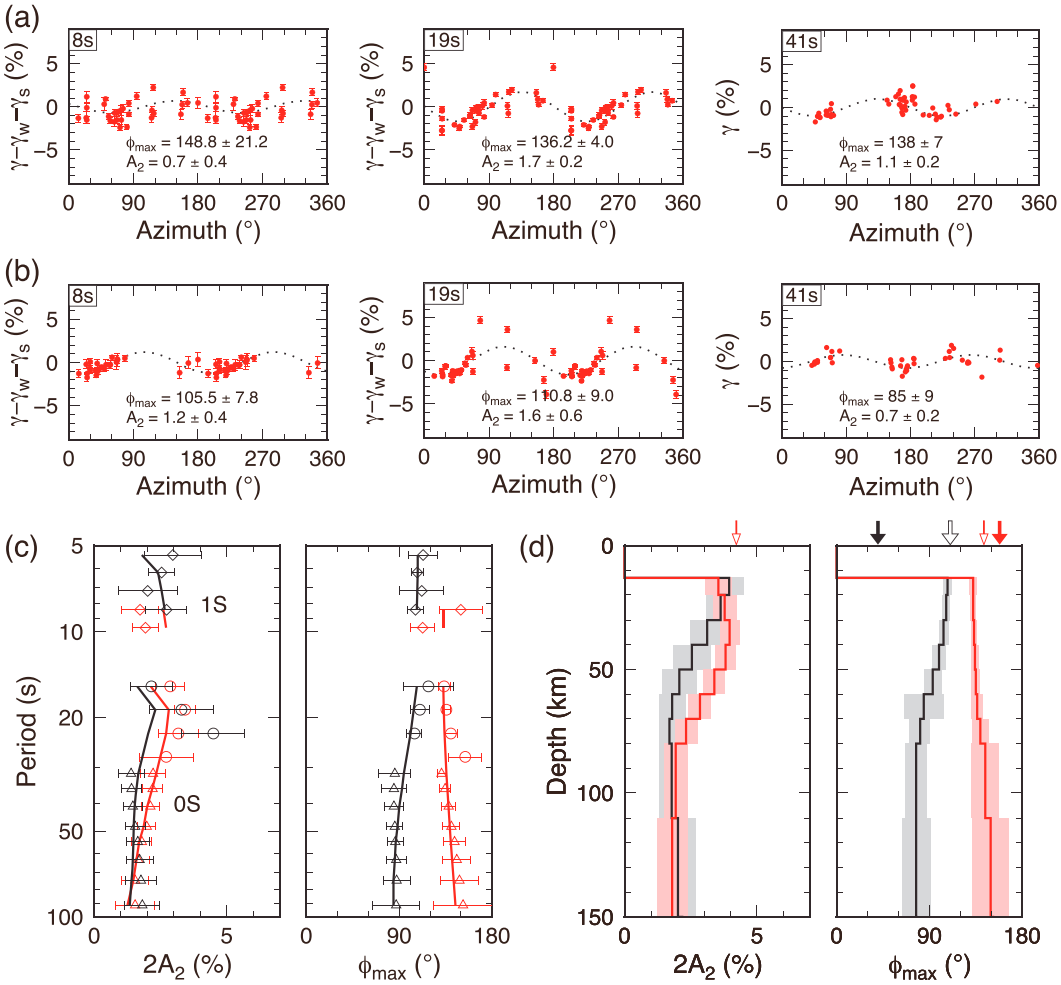

Figure 3. (a) Azimuthal dependence of phase velocity anomalies, γ, of Rayleigh waves in area A at periods of 8 s (1S mode) and 19 s (0S mode) obtained from ambient noise and at a period of 41 s (0S mode) obtained from teleseismic surface waves. The red dots are measurements. The dotted lines are fitting lines. The effect of water depth, γ_w, and source heterogeneity of ambient noise, γ_s, are subtracted from anomalies at periods of 8 and 19 s (see detail in Takeo et al., 2016). (b) Those in area B. (c) Peak-to-peak intensity, $2A_2$, and the fastest azimuth, ϕ_{max}, of the azimuthal dependence of phase velocities in each area. The red and black colors correspond to areas A and B, respectively. (d) One-dimensional profiles of β_V azimuthal anisotropy in each area. The three thick arrows on top correspond to the azimuths perpendicular to magnetic lineations in areas A (red filled) and B (black filled) and the azimuths of current plate motion (white filled). Thin white-filled red arrows indicate the refraction survey result of Shinohara et al. (2008) for sub-Moho anisotropy.

rotated to WSW-ENE in the LVZ in area B (Figures 1 and 3d). Both the strength (3.5%) and the fast direction (~130°N) of azimuthal anisotropy in the sub-Moho mantle of area A are generally consistent with the results of the active source Sn measurements (4.2% and 143°N) conducted at the eastern edge of the area by Shinohara et al. (2008), although the fast direction is slightly rotated counter-clockwise toward the current plate motion direction from the ancient spreading direction inferred from the magnetic lineations. The fast directions (~105°N) of area B exhibit no simple association either with the magnetic lineation or with the current plate motion.

4. Discussions

4.1. One-Dimensional Profile: Lid-to-LVZ Transition

The largest change of β_V occurs around a depth range of 60–80 km in the studied areas. It is of great interest to compare such in situ direct measurements with the results of global tomography; for example, Burgos et al. (2014) report, for Pacific Ocean sea-floors of crustal ages around 137.5 Ma, corresponding depths of ~120 ± 10 km that are far too large compared with our measurements. It indicates that the usage of the

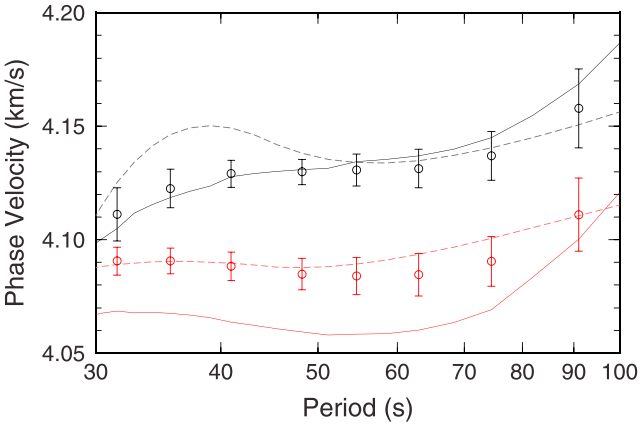

Figure 4. Comparison of the average phase-velocity measurements by the one-dimensional model-based approach of this study with correction of azimuthal anisotropy (circles) to those without correction of azimuthal anisotropy (solid lines) and by B-spline expansion with correction of azimuthal anisotropy (dashed lines) for areas A (red) and B (black).

depth derivatives of global tomographic models to infer the physical condition of the LAS in the ocean needs to be carefully conducted and that importance of incorporating regional measurements into large-scale tomographic modeling to advance our understanding of the LAS beneath the ocean (e.g., Kawakatsu & Utada, 2017).

Although surface wave dispersion measurements alone cannot constrain the depth interval of these changes, if they occur within an interval smaller than 30 km, G-discontinuity might be observed from body-wave analyses. In fact a velocity reduction of ~5% occurs in the depth range of 60–80 km that is comparable, though slightly smaller and shallower, to the reported G-discontinuity estimates via RF analysis (~80–85 km and 7–8%) by Kawakatsu et al. (2009) and Kumar et al. (2011) beneath the northeastern edge of area A. Since surface-wave dispersion curves are less sensitive to the gradient of boundary, model with such a sharp velocity boundary can also fit the dispersion curves in area A. In area B, however, such a strong discontinuity unlikely explains the dispersion curve. We thus consider that a significant G-discontinuity can only exist beneath area A.

4.2. One-Dimensional Profile: Regional Variation of LAS

While the Lid profiles are quite similar and indistinguishable within the model uncertainty between two areas, the difference between areas A and B in the LVZ is well resolved. The phase velocity of the fundamental-mode Rayleigh wave in area B is 1.5% faster than that in area A at periods of 40–100 s (Figure 2a). As a result, the β_V value in area A is estimated to be ~2% lower than that in area B (Figure 2b) in a depth range of 80–150 km in the LVZ. Although a similar pattern of β_V variation in two areas in the Lid and/or LVZ can be recognized in recent tomography models with horizontal resolutions of ~1,000 km (Burgos et al., 2014; Debayle & Ricard, 2013; Schaeffer & Lebedev, 2013), we could constrain the variation quantitatively without horizontal smoothing in this study because we used records directly above each area independently; in addition, we could constrain the depth of variation much better because we reduced the trade-off between Lid and LVZ velocities by analyzing surface waves at periods shorter than 30 s in the ambient noise.

The velocity difference of 2% in the asthenosphere corresponds to a temperature difference of ~250 K assuming the pyrolite model (Stixrude & Lithgow-Bertelloni, 2005, 2011). To evaluate whether this difference can be explained by the small difference in seafloor ages, we calculated synthetic dispersion curves for several thermal models of oceanic uppermost mantle including half-space with a potential temperature of 1,350 °C and a plate-cooling model with a plate thickness of 125 km and a potential temperature of 1,350 °C (Parsons & Sclater, 1977). The adiabatic temperature gradient is also introduced with a gradient of 0.3 K/km. We first construct vertical shear-wave velocity structures (Figure 5a) by using the pyrolite model. The pyrolite model is based on experimental results and gives average shear-wave velocity, $V_S = (\beta_V + \beta_H)/2$, where β_H and β_V models can be obtained from Love and Rayleigh waves, respectively. Since there is no Love-wave measurement in this study, we assumed the intensity of radial anisotropy to be 4% ($\beta_H/\beta_V = 1.04$) from Moho to a depth of 225 km. We also fixed the seismic attenuation structure to that of a global standard seismic model (PREM; Dziewonski & Anderson, 1981). As shown by results in Figure 5b, the observed phase velocities in area B could be fitted by the half-space cooling model, whereas those in area A could be fitted by the plate-cooling model. Although these results are under the strong assumptions of seismic radial anisotropy and seismic attenuation described above, we emphasize that neither of two thermal models could fit dispersion curves in two areas simultaneously and therefore that the small difference in the seafloor ages is not enough to produce the large velocity difference of ~2% in the LVZ.

One possible cause of the difference is the effect of the Shatsky Rise formed at the northern tip of the young Pacific Plate at 127–146 Ma (Nakanishi et al., 1999) that might have caused thermal and chemical alternation in the mantle beneath this region at the era. As explained below, however, both thermal and chemical anomalies seem difficult to create lateral heterogeneity only in the current LVZ, which we interpret as the asthenosphere. The thermal anomaly that created the thick crust of the Shatsky Rise should have

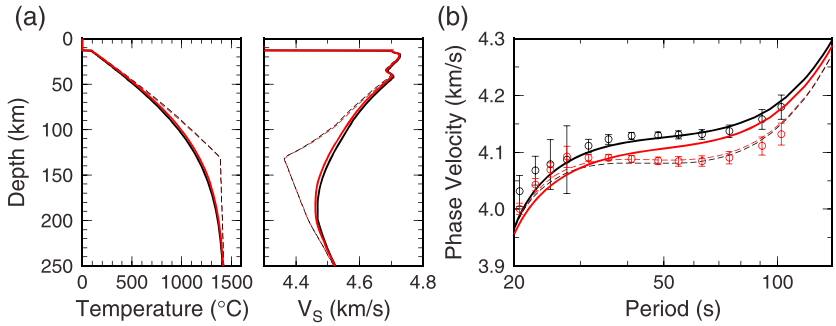

Figure 5. (a) Thermal models and corresponding V_S models for a half-space cooling model with a potential temperature of 1,350 °C (solid lines) and a plate-cooling model by Parsons and Sclater (1977) that has a potential temperature of 1,350 °C and plate thickness of 125 km (dashed lines). The seafloor ages are 130 Ma in area A (red) and 140 Ma in area B (black). (b) Phase-velocity measurements (circles) and model phase velocities corresponding to two thermal models (solid and dashed lines).

dissipated already. The chemical anomaly (Korenaga & Sager, 2012) can stay in the lithosphere, but not in the asthenosphere due to shear flow by the plate motion except for the case that the depleted viscous mantle has remained as a root of thick crust for more than 100 Ma. Such a high-velocity root has a potential of leaving ~1% anomaly of V_S (Schutt & Lesher, 2010). We consider that this interpretation is not likely because the intensity of anomaly is not enough to explain our observation of ~2%, and such an anomaly should be also seen in the current oceanic lithosphere. There is an observation of low-velocity root beneath Ontong Java plateau, but the sign of anomaly is opposite, and its origin is not yet fully understood (Richardson et al., 2000).

Another possible cause is the sublithospheric SSC predicted in the old oceanic uppermost mantle from the 1970s (e.g., Richter & Parsons, 1975). The SSC transfers heat from the deeper mantle to the bottom of the lithosphere, reheats, and creates small-scale lateral heterogeneity in the LVZ. Since dispersion curves in area A can be fitted by the plate-cooling model, reheating beneath LVZ seems to have occurred or been occurring now. In area B, the uppermost mantle might have been cooled only by conduction for 140 Ma as discussed by Korenaga and Korenaga (2008) for entire oceanic mantle without the anomalous crust, or convection might be also occurring in a manner that does not alter the thermal profile significantly. One simple interpretation is that a current downwelling exists beneath area B and is observed as a thermal profile cooler than the averaged profile of conductive mantle represented by the plate-cooling model.

Electrical conductivity profiles in two areas show a similar variation in a sense that the low conductivity layer, which is typically associated with Lid or lithosphere, is thicker in area B compared to area A (Baba et al., 2017). Integrated modeling of seismic and electrical signatures of the studied areas is currently in progress.

4.3. Anisotropy Profile (Lid/Lithosphere): Ancient Mantle Flow Oblique to Spreading Axis

The fastest azimuth of seismic anisotropy has been revealed to be perpendicular to magnetic lineations for several areas around the Shatsky Rise (Figure 1) both at the sub-Moho depth (Shinohara et al., 2008; Takeo et al., 2014) and at deeper depths of ~50–80 km (Shintaku et al., 2014). Oikawa et al. (2010) also examined two lines of seismic survey and concluded that the line perpendicular to magnetic lineation is faster at the southwest of the Shatsky Rise.

In area A, the intensity and the fastest azimuth of azimuthal anisotropy at depths shallower than 20 km of this study are consistent with the result of seismic refraction survey by Shinohara et al. (2008). The fastest azimuth is subparallel to the azimuth perpendicular to magnetic lineations (Figure 1). This result roughly agrees with the conventional view that the mantle flow perpendicular to the ridge axis aligns olivine crystals, frozen in the lithosphere, and is observed as the fastest azimuth parallel to the spreading direction inferred from the strike of transform fault (Raitt et al., 1971) or from the azimuth perpendicular to magnetic lineations (e.g., Smith et al., 2004). The slight difference between the fastest azimuth and the spreading direction is also observed in the Eastern Pacific Rise (Toomey et al., 2007).

In area B, on the other hand, the fastest azimuth at depths shallower than 20 km is oblique to the spreading direction by ~70° and inconsistent with the conventional view. In the south Pacific Ocean, azimuthal anisotropy in the lithosphere is also observed to be oblique to the azimuths perpendicular to magnetic lineations by ~50°, but parallel to the plate motion during seafloor spreading (Takeo et al., 2016); the discrepancy is created because the magnetic lineations are formed by Pacific-Farallon spreading at 60 Ma, whereas the plate motion during the seafloor spreading was mostly governed by faster Pacific-Antarctic spreading. Similarly, at 140 Ma when seafloor in area B is formed, the mantle flow might have been very complex; the seafloor spreading process of the old Pacific Plate at seafloor ages greater than 100 Ma might be different from the current one because of the complication due to the Pacific Plate being surrounded by three ridge axes with three different old oceanic plates: the Izanagi Plate at the northwest, the Farallon Plate at the northeast, and the Phoenix Plate at the south (Nakanishi et al., 1989, 1992, 1999). Due to the three ridges around the Pacific Plate and additional three ridges between those old oceanic plates, the tectonics might be quite different from the conventional plate tectonics developed in the current Atlantic Ocean or the eastern Pacific Ocean where one strong ridge dominates.

Furthermore, the Shatsky Rise was created in 127–146 Ma at the triple junction of the Pacific, Izanagi, and Farallon plates. The horizontal radial flow from the Shatsky Rise due to the excess of vertical upwelling can also simultaneously explain fastest azimuths in areas A and B. To verify these interpretations, future study about the numerical simulation of the six-ridge system is needed. The comparison between simulation results and observations, such as spreading rates and anisotropy fastest azimuths, may reveal the mantle dynamics beneath the infant Pacific Plate.

4.4. Anisotropy Profile (LVZ/Asthenosphere): Support for Sublithospheric SSC?

Our in situ measurement of azimuthal anisotropy for the LVZ offers the first direct such estimates in NW Pacific where the global tomography often gives a good fit with the prediction from the plate motion direction (e.g., Becker et al., 2014; Debayle & Ricard, 2013; Montagner, 1985; Tanimoto & Anderson, 1984). Results shown in Figures 1 and 3 indicate that, at deeper depths, the fastest azimuths slightly rotates clockwise compared to shallower depths in area A and anticlockwise in area B and that the observed fast directions do not coincide with those of the absolute plate motion, indicating that the mantle flow history in the asthenosphere is more complicated. van Hunen and Čadek (2009) showed that sublithospheric SSC that is expected to occur for the old LAS should result in the deviation of the fast direction from the large-scale flow direction dictated by the plate motion. Together with the large difference in the 1-D isotropic profiles in two areas, we suggest that our observation might indicate the first direct evidence for the occurrence of SSC beneath the old NW Pacific Ocean. It should be noted that the averaged azimuth between two areas roughly gives the azimuth of the current plate motion direction. Even under the existence of SSC, the tomographic image of azimuthal anisotropy in lower resolution might give fastest azimuths parallel to the plate motion direction as the conventional view.

4.5. Anisotropy Profile: Intensity

The intensity of azimuthal anisotropy is stronger at depths above 40–50 km in Lid than that at deeper depths both in areas A and B. The similar intensity reduction with depth is observed in other parts of Pacific from seafloor array experiments (Lin et al., 2016; Takeo et al., 2016). The strong azimuthal anisotropy at the shallow part is consistent with the observed strong Pn and Sn anisotropies by seismic refraction surveys (Raitt et al., 1971; Shinohara et al., 2008). The weaker azimuthal anisotropy at the deeper part is also consistent with tomography results, although the absolute intensity depends on the choice of damping parameters (Smith et al., 2004).

One possible cause of the vertical variation in the intensity is the strain accumulation at the top of asthenosphere near the ridge that is frozen in the lithosphere. The strong (~4%) radial anisotropy observed in the LVZ (Nettles & Dziewonski, 2008), however, suggests that the intensity of azimuthal anisotropy is smaller than that of radial anisotropy. The stronger radial anisotropy in the LVZ is inconsistent with A-type olivine crystals that have similar intensity of azimuthal and radial anisotropy (Crampin, 1977) and might be formed by the layering structure (e.g., Kawakatsu et al., 2009) and/or the AG-type olivine (Mainprice, 2007; Song & Kawakatsu, 2012, 2013). For more detailed discussion, we need to evaluate the effect of higher mode to the Love-wave dispersion curve and estimate radial anisotropy beneath each array in the future.

5. Summary

We analyzed records of 18 BBOBSs deployed at two arrays in the northwestern Pacific Ocean near the Shatsky Rise by the NOMan project. At a period range of 5–30 s, we extracted the fundamental- and the first higher-mode Rayleigh waves in ambient noise by cross-correlating continuous seismograms. In a period range of 30–100 s, we analyzed teleseismic Rayleigh waves. For each method, we obtained average dispersion curves and its azimuthal dependence for each array, which are then used to obtain one-dimensional isotropic and azimuthally anisotropic β_V profiles beneath each array. The obtained isotropic profiles have a gradual velocity drop at depths between 60 and 80 km that corresponds to the transition from the Lid to the LVZ. The estimated β_V value in the Lid is ~4.65 km/s both in areas A and B. The value in the LVZ is ~4.4 km/s in area A and ~4.5 km/s in area B. This difference cannot be explained by the small difference in the seafloor ages: 130 Ma in area A and 140 Ma in area B. Additional forward dispersion-curve calculation for several thermal models revealed that the structure beneath area A is consistent with the plate-cooling model, whereas that beneath area B is consistent with the half-space cooling model. This result suggests that the SSC might have reheated the bottom of oceanic lithosphere in area A. The fastest azimuths of azimuthal anisotropy in the LVZ significantly deviate from the current plate motion direction that is also consistent with the presence of sub-lithospheric SSC beneath the study area. The fastest azimuth of azimuthal anisotropy in the Lid is almost perpendicular to magnetic lineations in area A, while it is significantly oblique in area B. This result suggests the complexity of the mantle flow direction beneath area B in the past due to interactions between six ridge axes during the infancy of the Pacific plate. The intensity of azimuthal anisotropy in the LVZ is ~2% peak-to-peak, indicating that radial anisotropy is stronger than azimuthal anisotropy therein.

Acknowledgments
We thank the captain and crew of R/V *Kairei* and ROV Kaiko 7KII operated by JAMSTEC and researchers deployed BBOBSs: K. Miyakawa and T. Tonegawa. We also thank L. Stixrude, C. Lithgow-Bertelloni, and K. Baba for providing data to calculate thermal models. Two anonymous reviewers gave us helpful comments to improve the manuscript. This research was supported by JSPS KAKENHI grants JP22000003, 15K13558 and 18H03735. Original BBOBS records are archived in the Ocean Hemisphere Project Data Management Center (http://ohpdmc.eri.u-tokyo.ac.jp/) of Earthquake Research Institute, the University of Tokyo. We used GMT software (Wessel & Smith, 1991) to create figures.

References

Baba, K., Tada, N., Matsuno, T., Liang, P., Li, R., Zhang, L., et al. (2017). Electrical conductivity of old oceanic mantle in the northwestern Pacific I: 1-D profiles suggesting differences in thermal structure not predictable from a plate cooling model. *Earth, Planets and Space*, *69*(1), 111. https://doi.org/10.1186/s40623-017-0697-0

Baba, K., Tada, N., Zhang, L., Liang, P., Shimizu, H., & Utada, H. (2013). Is the electrical conductivity of the northwestern Pacific upper mantle normal? *Geochemistry, Geophysics, Geosystems*, *14*, 4969–4979. https://doi.org/10.1002/2013GC004997

Bagley, B., & Revenaugh, J. (2008). Upper mantle seismic shear discontinuities of the Pacific. *Journal of Geophysical Research*, *113*, B12301. https://doi.org/10.1029/2008JB005692

Becker, T. W., Conrad, C. P., Schaeffer, A. J., & Lebedev, S. (2014). Origin of azimuthal seismic anisotropy in oceanic plates and mantle. *Earth and Planetary Science Letters*, *401*, 236–250. https://doi.org/10.1016/j.epsl.2014.06.014

Burgos, G., Montagner, J.-P., Beucler, E., Capdeville, Y., Mocquet, A., & Drilleau, M. (2014). Oceanic lithosphere-asthenosphere boundary from surface wave dispersion data. *Journal of Geophysical Research: Solid Earth*, *119*, 1079–1093. https://doi.org/10.1002/2013JB010528

Cara, M., & Leveque, J. (1987). Waveform inversion using secondary observables. *Geophysical Research Letters*, *14*(10), 1046–1049. https://doi.org/10.1029/GL014i010p01046

Crampin, S. (1977). A review of the effects of anisotropic layering on the propagation of seismic waves. *Geophysical Journal International*, *49*(1), 9–27. https://doi.org/10.1111/j.1365-246X.1977.tb03698.x

Davis, E. E., & Lister, C. R. B. (1974). Fundamentals of ridge crest topography. *Earth and Planetary Science Letters*, *21*(4), 405–413. https://doi.org/10.1016/0012-821X(74)90180-0

Debayle, E., & Ricard, Y. (2013). Seismic observations of large-scale deformation at the bottom of fast-moving plates. *Earth and Planetary Science Letters*, *376*, 165–177. https://doi.org/10.1016/j.epsl.2013.06.025

Dziewonski, A. M., & Anderson, D. L. (1981). Preliminary reference Earth model. *Physics of the Earth and Planetary Interiors*, *25*(4), 297–356. https://doi.org/10.1016/0031-9201(81)90046-7

Forsyth, D. W., & Li, A. (2005). Array analysis of two-dimensional variations in surface wave phase velocity and azimuthal anisotropy in the presence of Multipathing interference. In A. Levander, & G. Nolet (Eds.), *Seismic Earth: Array analysis of broadband seismograms* (pp. 81–97). Washington, DC: American Geophysical Union.

Foster, A., Nettles, M., & Ekstrom, G. (2014). Overtone interference in array-based love-wave phase measurements. *Bulletin of the Seismological Society of America*, *104*(5), 2266–2277. https://doi.org/10.1785/0120140100

Gaherty, J. B., Jordan, T. H., & Gee, L. S. (1996). Seismic structure of the upper mantle in a Central Pacific corridor. *Journal of Geophysical Research*, *101*(B10), 22291–22309. https://doi.org/10.1029/96JB01882

Harmon, N., Forsyth, D., & Webb, S. (2007). Using ambient seismic noise to determine short-period phase velocities and shallow shear velocities in young oceanic lithosphere. *Bulletin of the Seismological Society of America*, *97*(6), 2009–2023. https://doi.org/10.1785/0120070050

Harmon, N., Forsyth, D., & Weeraratne, D. (2009). Thickening of young Pacific lithosphere from high-resolution Rayleigh wave tomography: A test of the conductive cooling model. *Earth and Planetary Science Letters*, *278*(1–2), 96–106. https://doi.org/10.1016/j.epsl.2008.11.025

Huang, J., & Zhong, S. (2005). Sublithospheric small-scale convection and its implications for the residual topography at old ocean basins and the plate model. *Journal of Geophysical Research*, *110*, B05404. https://doi.org/10.1029/2004JB003153

Kawakatsu, H. (2016). A new fifth parameter for transverse isotropy. *Geophysical Journal International*, *204*(1), 682–685. https://doi.org/10.1093/gji/ggv479

Kawakatsu, H., Kumar, P., Takei, Y., Shinohara, M., Kanazawa, T., Araki, E., & et al. (2009). Seismic evidence for sharp lithosphere-asthenosphere boundaries of oceanic plates. *Science*, *324*(5926), 499–502. https://doi.org/10.1126/science.1169499

Kawakatsu, H., & Utada, H. (2017). Seismic and electrical signatures of the lithosphere–asthenosphere system of the normal oceanic mantle. *Annual Review of Earth and Planetary Sciences*, *45*(1), 139–167. https://doi.org/10.1146/annurev-earth-063016-020319

Korenaga, J., & Sager, W. W. (2012). Seismic tomography of Shatsky Rise by adaptive importance sampling. *Journal of Geophysical Research*, *117*, B08102. https://doi.org/10.1029/2012JB009248
Korenaga, T., & Korenaga, J. (2008). Subsidence of normal oceanic lithosphere, apparent thermal expansivity, and seafloor flattening. *Earth and Planetary Science Letters*, *268*(1–2), 41–51. https://doi.org/10.1016/j.epsl.2007.12.022
Kumar, P., & Kawakatsu, H. (2011). Imaging the seismic lithosphere-asthenosphere boundary of the oceanic plate. *Geochemistry, Geophysics, Geosystems*, *12*, Q01006. https://doi.org/10.1029/2010GC003358
Kumar, P., Kawakatsu, H., Shinohara, M., Kanazawa, T., Araki, E., & Suyehiro, K. (2011). P and S receiver function analysis of seafloor borehole broadband seismic data. *Journal of Geophysical Research*, *116*, B12308. https://doi.org/10.1029/2011JB008506
Lin, P. P., Gaherty, J. B., Jin, G., Collins, J. A., Lizarralde, D., Evans, R. L., & et al. (2016). High-resolution seismic constraints on flow dynamics in the oceanic asthenosphere. *Nature*, *535*(7613), 538–541. https://doi.org/10.1038/nature18012
Maggi, A., Debayle, E., Priestley, K., & Barruol, G. (2006a). Multimode surface waveform tomography of the Pacific Ocean: A closer look at the lithospheric cooling signature. *Geophysical Journal International*, *166*(3), 1384–1397. https://doi.org/10.1111/j.1365-246X.2006.03037.x
Maggi, A., Debayle, E., Priestley, K., & Barruol, G. (2006b). Azimuthal anisotropy of the Pacific region. *Earth and Planetary Science Letters*, *250*(1–2), 53–71. https://doi.org/10.1016/j.epsl.2006.07.010
Mainprice, D. (2007). Seismic anisotropy of the deep earth from a mineral and rock physics perspective. *Treatise on Geophysics*, *2*, 437–492. https://doi.org/10.1016/B978-044452748-6/00045-6
Matsuno, T., Suetsugu, D., Baba, K., Tada, N., Shimizu, H., Shiobara, H., et al. (2017). Mantle transition zone beneath a normal seafloor in the northwestern Pacific: Electrical conductivity, seismic thickness, and water content. *Earth and Planetary Science Letters*, *462*, 189–198. https://doi.org/10.1016/j.epsl.2016.12.045
Montagner, J.-P. (1985). Seismic anisotropy of the Pacific Ocean inferred from long-period surface waves dispersion. *Physics of the Earth and Planetary Interiors*, *38*(1), 28–50. https://doi.org/10.1016/0031-9201(85)90120-7
Müller, R. D., Sdrolias, M., Gaina, C., & Roest, W. R. (2008). Age, spreading rates, and spreading asymmetry of the world's ocean crust. *Geochemistry, Geophysics, Geosystems*, *9*, Q04006. https://doi.org/10.1029/2007GC001743
Nakanishi, M., Sager, W. W., & Klaus, A. (1999). Magnetic lineations within Shatsky Rise, Northwest Pacific Ocean: Implications for hot spot-triple junction interaction and oceanic plateau formation. *Journal of Geophysical Research*, *104*(B4), 7539–7556. https://doi.org/10.1029/1999JB900002
Nakanishi, M., Tamaki, K., & Kobayashi, K. (1989). Mesozoic magnetic anomaly lineations and seafloor spreading history of the northwestern Pacific. *Journal of Geophysical Research*, *94*(B11), 15,437–15,462. https://doi.org/10.1029/JB094iB11p15437
Nakanishi, M., Tamaki, K., & Kobayashi, K. (1992). Magnetic anomaly lineations from Late Jurassic to Early Cretaceous in the west-central Pacific Ocean. *Geophysical Journal International*, *109*(3), 701–719. https://doi.org/10.1111/j.1365-246X.1992.tb00126.x
Nettles, M., & Dziewonski, A. M. (2008). Radially anisotropic shear velocity structure of the upper mantle globally and beneath North America. *Journal of Geophysical Research*, *113*, B02303. https://doi.org/10.1029/2006JB004819
Nishimura, C. E., & Forsyth, D. W. (1988). Rayleigh wave phase velocities in the Pacific with implications for azimuthal anisotropy and lateral heterogeneities. *Geophysical Journal*, *94*(3), 479–501. https://doi.org/10.1111/j.1365-246X.1988.tb02270.x
Oikawa, M., Kaneda, K., & Nishizawa, A. (2010). Seismic structures of the 154–160 Ma oceanic crust and uppermost mantle in the Northwest Pacific Basin. *Earth, Planets and Space*, *62*(4), e13–e16. https://doi.org/10.5047/eps.2010.02.011
Parsons, B., & Sclater, J. G. (1977). An analysis of the variation of ocean floor bathymetry and heat flow with age. *Journal of Geophysical Research*, *82*(5), 803–827. https://doi.org/10.1029/JB082i005p00803
Raitt, R. W., Shor, G. G., Morris, G. B., & Kirk, H. K. (1971). Mantle anisotropy in the Pacific Ocean. *Tectonophysics*, *12*(3), 173–186. https://doi.org/10.1016/0040-1951(71)90002-3
Revenaugh, J., & Jordan, T. H. (1991). Mantle layering from ScS reverberations: 3. The upper mantle. *Journal of Geophysical Research*, *96*(B12), 19781–19810. https://doi.org/10.1029/91JB01487
Richardson, W. P., Okal, E. A., & van der Lee, S. (2000). Rayleigh-wave tomography of the Ontong-Java Plateau. *Physics of the Earth and Planetary Interiors*, *118*(1–2), 29–51. https://doi.org/10.1016/S0031-9201(99)00122-3
Richter, F. M., & Parsons, B. (1975). On the interaction of two scales of convection in the mantle. *Journal of Geophysical Research*, *80*(17), 2529–2541. https://doi.org/10.1029/JB080i017p02529
Ritzwoller, M. H., Shapiro, N. M., & Zhong, S.-J. (2004). Cooling history of the Pacific lithosphere. *Earth and Planetary Science Letters*, *226*(1-2), 69–84. https://doi.org/10.1016/j.epsl.2004.07.032
Rychert, C. A., & Shearer, P. M. (2011). Imaging the lithosphere-asthenosphere boundary beneath the Pacific using SS waveform modeling. *Journal of Geophysical Research*, *116*, B07307. https://doi.org/10.1029/2010JB008070
Schaeffer, A. J., & Lebedev, S. (2013). Global shear speed structure of the upper mantle and transition zone. *Geophysical Journal International*, *194*(1), 417–449. https://doi.org/10.1093/gji/ggt095
Schutt, D. L., & Lesher, C. E. (2010). Compositional trends among Kaapvaal Craton garnet peridotite xenoliths and their effects on seismic velocity and density. *Earth and Planetary Science Letters*, *300*(3–4), 367–373. https://doi.org/10.1016/j.epsl.2010.10.018
Shapiro, N. M., & Campillo, M. (2004). Emergence of broadband Rayleigh waves from correlations of the ambient seismic noise. *Geophysical Research Letters*, *31*, L07614. https://doi.org/10.1029/2004GL019491
Shinohara, M., Fukano, T., Kanazawa, T., Araki, E., Suyehiro, K., Mochizuki, M., et al. (2008). Upper mantle and crustal seismic structure beneath the northwestern Pacific Basin using a seafloor borehole broadband seismometer and ocean bottom seismometers. *Physics of the Earth and Planetary Interiors*, *170*(1–2), 95–106. https://doi.org/10.1016/j.pepi.2008.07.039
Shintaku, N., Forsyth, D. W., Hajewski, C. J., & Weeraratne, D. S. (2014). Pn anisotropy in Mesozoic western Pacific lithosphere. *Journal of Geophysical Research: Solid Earth*, *119*, 3050–3063. https://doi.org/10.1002/2013JB010534
Shiobara, H., Kanazawa, T., & Isse, T. (2013). New step for broadband seismic observation on the sea floor: BBOBS-NX. *IEEE-JOE*, *38*(2), 396–405. https://doi.org/10.1109/JOE.2012.2222792
Smith, D. B., Ritzwoller, M. H., & Shapiro, N. M. (2004). Stratification of anisotropy in the Pacific upper mantle. *Journal of Geophysical Research*, *109*, B11309. https://doi.org/10.1029/2004JB003200
Song, T.-R. A., & Kawakatsu, H. (2012). Subduction of oceanic asthenosphere: Evidence from sub-slab seismic anisotropy. *Geophysical Research Letters*, *39*, L17301. https://doi.org/10.1029/2012GL052639
Song, T.-R. A., & Kawakatsu, H. (2013). Subduction of oceanic asthenosphere: A critical appraisal in Central Alaska. *Earth and Planetary Science Letters*, *367*, 82–94. https://doi.org/10.1016/j.epsl.2013.02.010
Stein, C. A., & Stein, S. (1992). A model for the global variation in oceanic depth and heat flow with lithospheric age. *Nature*, *359*(6391), 123–129. https://doi.org/10.1038/359123a0
Stixrude, L., & Lithgow-Bertelloni, C. (2005). Mineralogy and elasticity of the oceanic upper mantle: Origin of the low-velocity zone. *Journal of Geophysical Research*, *110*, B03204. https://doi.org/10.1029/2004JB002965

Stixrude, L., & Lithgow-Bertelloni, C. (2011). Thermodynamics of mantle minerals—II. Phase equilibria. *Geophysical Journal International*, *184*(3), 1180–1213. https://doi.org/10.1111/j.1365-246X.2010.04890.x

Suetsugu, D., & Shiobara, H. (2014). Broadband ocean-bottom seismology. *Annual Review of Earth and Planetary Sciences*, *42*(1), 27–43. https://doi.org/10.1146/annurev-earth-060313-054818

Takeo, A., Forsyth, D. W., Weeraratne, D. S., & Nishida, K. (2014). Estimation of azimuthal anisotropy in the NW Pacific from seismic ambient noise in seafloor records. *Geophysical Journal International*, *199*(1), 11–22. https://doi.org/10.1093/gji/ggu240

Takeo, A., Kawakatsu, H., Isse, T., Nishida, K., Sugioka, H., Ito, A., et al. (2016). Seismic azimuthal anisotropy in the oceanic lithosphere and asthenosphere from broadband surface wave analysis of OBS array records at 60 Ma seafloor. *Journal of Geophysical Research*, *121*, 1927–1947. https://doi.org/10.1002/2015JB012429

Takeo, A., Nishida, K., Isse, T., Kawakatsu, H., Shiobara, H., Sugioka, H., & et al. (2013). Radially anisotropic structure beneath the Shikoku Basin from broadband surface wave analysis of ocean bottom seismometer records. *Journal of Geophysical Research*, *118*, 2878–2892. https://doi.org/10.1002/jgrb.50219

Takeuchi, H., & Saito, M. (1972). Seismic surface waves. In B. A. Bolt (Ed.), *Methods in computational physics* (pp. 217–295). New York: Academic Press.

Takeuchi, N., Kawakatsu, H., Shiobara, H., Isse, T., Sugioka, H., Ito, A., & et al. (2017). Determination of intrinsic attenuation in the oceanic lithosphere-asthenosphere system. *Science*, *358*(6370), 1593–1596. https://doi.org/10.1126/science.aao3508

Tanimoto, T., & Anderson, D. L. (1984). Mapping convection in the mantle. *Geophysical Research Letters*, *11*(4), 287–290. https://doi.org/10.1029/GL011i004p00287

Tonegawa, T., Fukao, Y., Takahashi, T., Obana, K., Kodaira, S., & Kaneda, Y. (2015). Ambient seafloor noise excited by earthquakes in the Nankai subduction zone. *Nature Communications*, *6*(1), 6132. https://doi.org/10.1038/ncomms7132

Toomey, D. R., Jousselin, D., Dunn, R. A., Wilcock, W. S. D., & Detrick, R. S. (2007). Skew of mantle upwelling beneath the East Pacific Rise governs segmentation. *Nature*, *446*(7134), 409–414. https://doi.org/10.1038/nature05679

van Hunen, J., & Čadek, O. (2009). Reduced oceanic seismic anisotropy by small-scale convection. *Earth and Planetary Science Letters*, *284*(3–4), 622–629. https://doi.org/10.1016/j.epsl.2009.05.034

Vine, F. J., & Matthews, D. H. (1963). Magnetic anomalies over oceanic ridges. *Nature*, *199*(4897), 947–949. https://doi.org/10.1038/199947a0

Wessel, P., & Smith, W. H. F. (1991). Free software helps map and display data. *Eos, Transactions American Geophysical Union*, *72*(41), 441–441. https://doi.org/10.1029/90EO00319

Yao, H., Gouédard, P., Collins, J. A., McGuire, J. J., & van der Hilst, R. D. (2011). Structure of young East Pacific Rise lithosphere from ambient noise correlation analysis of fundamental- and higher-mode Scholte-Rayleigh waves. *Comptes Rendus Geoscience*, *343*(8-9), 571–583. https://doi.org/10.1016/j.crte.2011.04.004

Yoshizawa, K. (2014). Radially anisotropic 3-D shear wave structure of the Australian lithosphere and asthenosphere from multi-mode surface waves. *Physics of the Earth and Planetary Interiors*, *235*, 33–48. https://doi.org/10.1016/j.pepi.2014.07.008